


## Strongly Enhanced Berry Dipole at Topological Phase Transitions in BiTeI

Jorge I. Facio,<sup>1</sup> Dmitri Efremov,<sup>1</sup> Klaus Koepf, <sup>1</sup> Jih-Shih You,<sup>1</sup> Inti Sodemann,<sup>2</sup> and Jeroen van den Brink<sup>1,3</sup>

<sup>1</sup>*Institute for Theoretical Solid State Physics, IFW Dresden, Helmholtzstr. 20, 01069 Dresden, Germany*

<sup>2</sup>*Max Planck Institute for the Physics of Complex Systems, Nöthnitzerstr. 38, 01187 Dresden, Germany*

<sup>3</sup>*Department of Physics, Technical University Dresden, Helmholtzstr. 10, 01062 Dresden, Germany*

 (Received 25 May 2018; published 14 December 2018)

Transitions between topologically distinct electronic states have been predicted in different classes of materials and observed in some. A major goal is the identification of measurable properties that directly expose the topological nature of such transitions. Here, we focus on the giant Rashba material bismuth tellurium iodine which exhibits a pressure-driven phase transition between topological and trivial insulators in three dimensions. We demonstrate that this transition, which proceeds through an intermediate Weyl semimetallic state, is accompanied by a giant enhancement of the Berry curvature dipole which can be probed in transport and optoelectronic experiments. From first-principles calculations, we show that the Berry dipole—a vector along the polar axis of this material—has opposite orientations in the trivial and topological insulating phases and peaks at the insulator-to-Weyl critical points, at which the nonlinear Hall conductivity can increase by over 2 orders of magnitude.

DOI: [10.1103/PhysRevLett.121.246403](https://doi.org/10.1103/PhysRevLett.121.246403)

A material that is on the verge of a transition between two phases is prone to strongly enhanced responses to small external perturbations. Such divergent susceptibilities are well-known for critical systems with thermal phase transitions in which the development of long-range order is characterized by a local order parameter. However, for systems that have a *topological* electronic phase transition, in which local order parameter physics is absent, the identification and characterization of measurable signatures of the topological change close to criticality remains largely an open problem. In this context, we investigate pressure-induced topological electronic phase transitions in the giant Rashba semiconductor bismuth tellurium iodine (BiTeI) [1]. This allows us to identify a direct experimental signature of the topological transition: a very strongly enhanced nonlinear Hall conductivity, which is related to a large increase of the Berry curvature dipole moment of the electronic bands close to criticality.

BiTeI is a trivial insulator with a strong Rashba-type spin-orbit coupling and has been predicted to become a strong topological insulator at moderate pressures [2]. These insulating phases are separated by an intermediate Weyl phase [3,4]. The ambient pressure crystalline structure has been demonstrated to be stable up to about 9 GPa, which is well above the theoretically expected pressure for the topological phase transition at about 3 GPa [5]. Although there are arguments based on optical experiments for the existence of the topological phase transition [6], the optical properties display a rather smooth evolution up to 9 GPa [7]. On the other hand, transport experiments present a broad minimum of resistivity at the pressures near where the topological phase transition is expected [5,8].

Therefore, to our knowledge, there is no experimental evidence of signatures directly associated with the topological nature of the phase transition, such as the appearance of metallic surface states.

A crucial property of BiTeI is the absence of inversion symmetry, which endows the Bloch states with a nonzero Berry curvature. This opens the possibility to analyze the transitions between the topologically distinct electronic phases by means of response functions that are particularly sensitive to the geometry of the Bloch states [9–16]. Recent experiments [17,18] have reported the observation of the time reversal invariant nonlinear Hall effect [9] in two-dimensional transition metal dichalcogenides [19–22]. Here, we demonstrate that such nonlinear Hall effect can also be a useful probe of a topological phase transition and establish BiTeI as a promising platform to experimentally observe this effect in three dimensions.

The associated Hall current that is *nonlinear* in the electric field originates from the anomalous velocity caused by the Berry curvature of the electronic bands. Specifically, in the presence of an electric field  $E_c = \text{Re}\{\mathcal{E}_c e^{i\omega t}\}$ , the second-order response current reads  $j_a = \text{Re}\{j_a^{(0)} + j_a^{(2\omega)} e^{2i\omega t}\}$ , where  $j_a^{(0)} = \chi_{abc} \mathcal{E}_b \mathcal{E}_c^*$  and  $j_a^{(2\omega)} = \chi_{abc} \mathcal{E}_b \mathcal{E}_c$ . The nonlinear response function  $\chi_{abc}$  effectively measures a *first-order moment* of the Berry curvature over the occupied states, the Berry dipole

$$\chi_{abc} = -\epsilon_{adc} \frac{e^3 \tau}{2(1 + i\omega\tau)} D_{bd}, \quad (1)$$

$$D_{bd} = \int \frac{d^3\mathbf{k}}{(2\pi)^3} \sum_n \Omega_{n,d}(\mathbf{k}) \left( -\frac{\partial f_0}{\partial E} \right)_{E=E_{n\mathbf{k}}} \frac{\partial E_{n\mathbf{k}}}{\partial k_b}. \quad (2)$$

Here,  $E_{n\mathbf{k}}$  is the energy dispersion of the  $n$ th band,  $f_0$  the equilibrium Fermi distribution,  $\tau$  the relaxation time, and  $\Omega_{n,d}$  is the  $d$  component of the Berry curvature,  $\Omega_n(\mathbf{k}) = \nabla_{\mathbf{k}} \times \mathbf{A}_n(\mathbf{k})$ , where  $\mathbf{A}_n(\mathbf{k}) = -i\langle u_{n\mathbf{k}} | \partial_{\mathbf{k}} u_{n\mathbf{k}} \rangle$ . In this Letter, we study the nonlinear Hall conductivity of BiTeI as a function of hydrostatic pressure by computing the Berry-dipole  $D$  from first principles. In addition, we present an analytical description of our main results based on a low-energy model and finally, we analyze transport and optoelectronic experiments that are expected to exhibit fingerprints of the Berry dipole.

**Topological phase transitions.**—BiTeI is a layered polar compound with space group  $P3m1$  (No. 156). Bi, Te, and I layers, each having  $C_{3v}$  symmetry, are stacked along the  $c$ -axis breaking inversion symmetry; see Fig. 1(a). To study the evolution under hydrostatic pressure ( $P$ ), we use the experimental values of the lattice parameters  $a$  and  $c$  reported in Ref. [6]. We also consider additional pressures in between the ones for which experimental data are available, interpolating  $a$  and  $c$  linearly from the experimental data. For fixed values of  $a$  and  $c$ , we determine the vertical position of the Te and I atoms by minimization of the total energy.

For each pressure, we perform fully relativistic density functional theory calculations [23] and compute the Berry curvature of the Bloch states by Wannier interpolation [25] [see the Supplemental Material [30]]. In three dimensions,

the Berry curvature is a vector field defined in the Brillouin zone. We find convenient to measure its components in cylindrical coordinates with the  $z$  axis along the polar axis of BiTeI, as shown in Fig. 1(b). Figures 1(c)–1(e) show for different pressures the band structure and the azimuthal component of the Berry curvature of the conducting bands ( $\Omega_\phi$ ). As we will see later, this is the component that contributes to the Berry dipole in BiTeI. The energy exhibits the Rashba-like dispersion, whereas  $\Omega_\phi$  has extremes at the bottom of the conduction bands. As  $P$  increases, the gap between valence and conduction bands ( $\Delta$ ) is reduced and the extreme of  $\Omega_\phi$  along the path  $AH$  becomes sharper and achieves larger values. The gap initially closes at  $P_{c1} = 2.9$  GPa in a point belonging to this path. Upon further increasing  $P$ , the Weyl nodes move both in  $k_y$  and  $k_z$  directions until they annihilate in the mirror plane  $AML$  and the gap reopens at  $P_{c2} = 3.0$  GPa. This evolution of the Weyl nodes is in agreement with previous calculations [3,4]. For  $P > P_{c2}$ , increasing the pressure pushes the system deep into the topological insulating phase and the maximum of the Berry curvature is reduced. Interestingly, because of the band inversion the Berry curvature has opposite sign in the two insulating states. Figure 1(f) sketches the phase diagram, showing  $\Delta$  as a function of  $P$ . The pressures in which  $\Delta$  vanishes are in excellent agreement with experimental expectations [5,6].

**Berry curvature dipole.**—We begin by considering how the  $C_{3v}$  symmetry constraints the Berry-dipole tensor. Figures 2(a) and 2(b) show  $\Omega$  in cylindrical coordinates for particular values of  $k_z$ . Because  $\Omega$  is a pseudovector, the

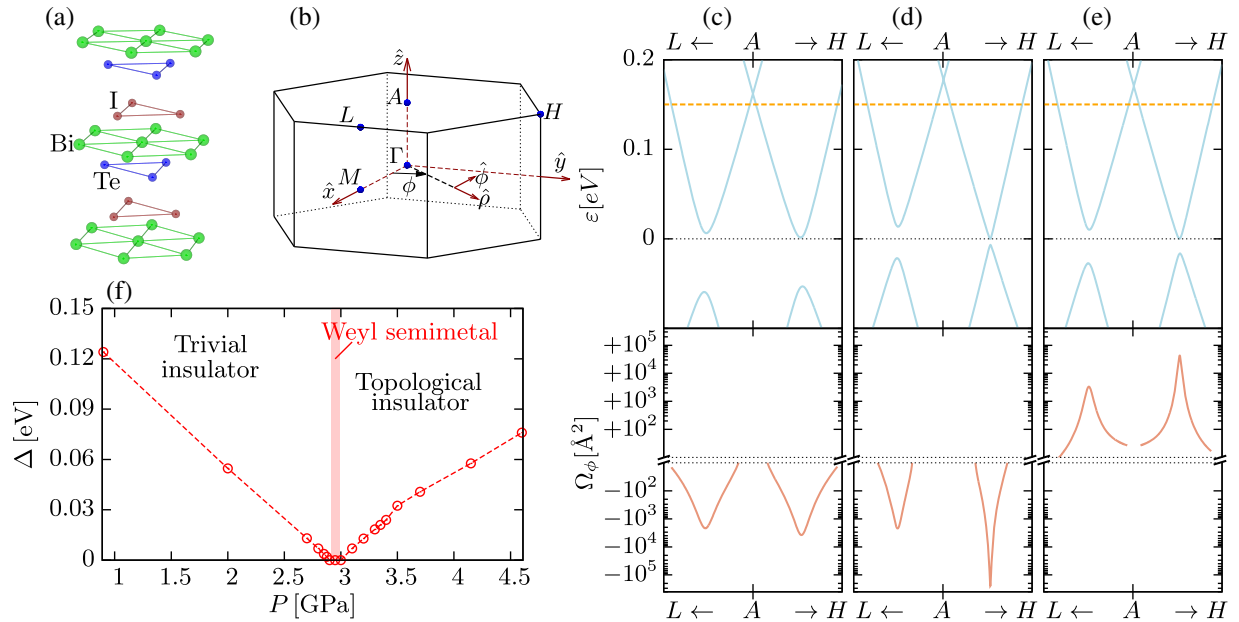


FIG. 1. (a) Crystal structure of BiTeI. (b) Brillouin zone. (c)–(e): Band structure (top) and azimuthal component of the total Berry curvature  $\Omega_\phi$  (bottom) for pressures  $P = 2.0, 2.8,$  and  $3.2$  GPa, respectively. The Berry curvature is that of the states in the conduction band, considering the chemical potential as indicated by the dotted orange line. (f) Energy gap between valence and conduction states as a function of pressure.

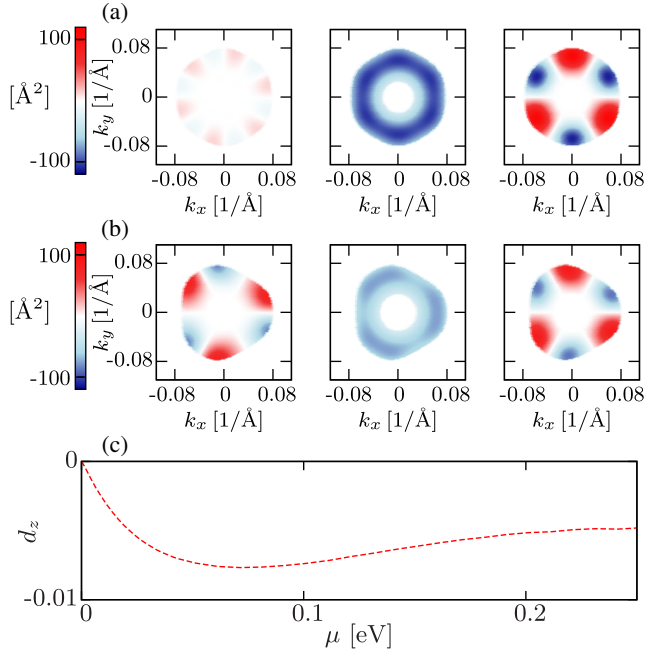


FIG. 2. Berry curvature and Berry dipole at ambient pressure. (a),(b): Berry curvature of the conducting states of momentum  $k_z = \pi/c$  and  $k_z = 0.9\pi/c$ , respectively.  $\Omega_\rho$ ,  $\Omega_\phi$ , and  $\Omega_z$  are shown from left to right.  $\Omega_\rho$  is magnified by a factor of 5. (c) Berry dipole as a function of the chemical potential.

components  $\Omega_\rho$  and  $\Omega_z$  are odd with respect to mirror planes, while  $\Omega_\phi$  is even. As a result, the azimuthal component is seen to swirl around the polar axis in a solenoidal fashion. This circulating pattern is what gives rise to a nonvanishing Berry dipole in BiTeI. On the other hand,  $\Omega_\rho$  and  $\Omega_z$  must change sign at the mirrors and their contributions average out to zero. As explained in Ref. [9], the existence of three mirror planes related by threefold rotations along the polar axis forces the symmetric part of  $D_{bd}$  to vanish. The remaining antisymmetric part can be described as a vector that lies along the polar axis. Therefore, we will focus on this vector which can be written in terms of Eq. (2) as  $\mathbf{d} = d_z \hat{z}$ , where  $d_z = (D_{xy} - D_{yx})/2$ .

Figure 2(c) presents  $d_z$  as a function of the chemical potential,  $\mu$ , at ambient pressure and zero temperature. Naturally, without doping ( $\mu = 0$ ),  $d_z$  vanishes because of the absence of carriers. The values obtained at finite doping are moderate as compared to the ones obtained in Ref. [36] for different Weyl semimetals and larger than found in Ref. [37] for trigonal tellurium. The maximum in absolute value as a function of  $\mu$  arises from the competition between the Berry curvature, which is larger at the band bottom, and the growing number of states as the chemical potential increases. Namely, the maximum corresponds to an electronic density that optimizes the compromise between giving rise to a large Fermi surface and having carriers at the Fermi level with large Berry curvature. For a

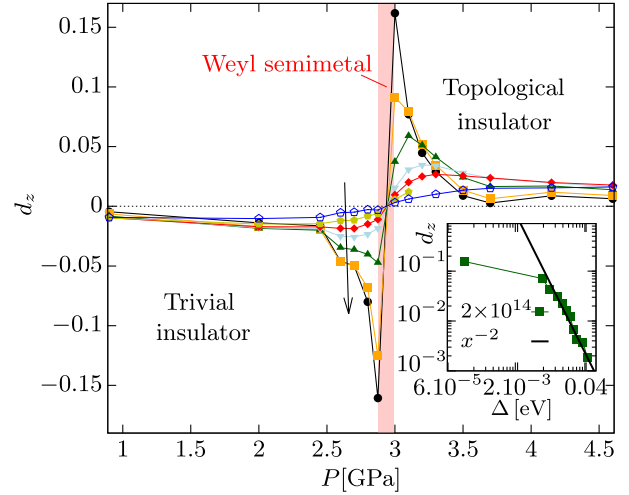


FIG. 3. Berry dipole as a function of pressure for fixed different values of density. The arrow indicates the direction of decreasing density, the different curves correspond to  $1 \times 10^{17}$ ,  $5 \times 10^{16}$ ,  $3 \times 10^{16}$ ,  $2 \times 10^{16}$ ,  $1 \times 10^{16}$ ,  $3 \times 10^{15}$ , and  $1 \times 10^{15} \text{ cm}^{-3}$ . Inset: Berry dipole as a function of  $\Delta$  in the limit of small density in the topological insulating phase.

fixed density, hydrostatic pressure can affect this competition by significantly increasing the Berry curvature of the states at the band bottom, as we discuss next.

Figure 3 presents the Berry dipole as a function of pressure for different electronic densities,  $n$ . One of the central findings of our Letter is that the Berry curvature dipole vector,  $\mathbf{d} = d_z \hat{z}$ , reverses its orientation in going from the trivial to the topological insulating phase. The origin of this reversal can be traced back to the band inversion that causes a change of sign in the Berry curvature (see Fig. 1) and, therefore, the measurement of the Berry dipole offers a direct signature of the topological nature of the phase transition. The evolution with pressure exhibits a noticeable dependence on the amount of doping. For large  $n$ , the carriers at the Fermi surface have relatively small Berry curvature and the evolution of  $d_z$  is rather smooth. As the density is reduced, the Fermi surface comes closer to the location of the Weyl nodes in the intervening semimetallic phase, giving rise to a large enhancement of the Berry curvature and its dipole. In this regime, the Berry dipole not only has a different sign in the two insulating phases but also displays sharp peaks located at the topological phase transitions. According to our calculations, this dependence on the density is observed up to  $n \sim 1 \times 10^{15} \text{ cm}^{-3}$ . Reducing further  $n$ , the decrease in the number of states becomes dominant and, as expected in the limit  $\mu \rightarrow 0$ ,  $d_z$  decreases its absolute value (see Ref. [30]).

*Model.*—We now introduce a low-energy model to analyze the behavior of the Berry dipole across the topological phase transitions. We first focus on the enhancement obtained when the Weyl phase is approached

from the topological insulator side. We consider a two-band model for the pair creation or annihilation of Weyl nodes near one of the mirror invariant planes [AML planes, see Fig. 1(b)]. The valence and conduction bands will touch at some point  $\mathbf{k}_0$  along this plane. The corresponding mirror is the only element of the little group. Choosing  $\hat{\mathbf{x}}$  along the AL line,  $\hat{\mathbf{y}}$  along LH, and  $\hat{\mathbf{z}}$  along  $\Gamma A$ , the mirror acts as

$$M: k_y \rightarrow -k_y, \quad k_{x,z} \rightarrow k_{x,z}. \quad (3)$$

A simple “k dot p” model capturing the symmetries and the pair creation of Weyl nodes is

$$H = \frac{(k_y^2 + \lambda)}{2m} \sigma_y + k_x v_x \sigma_x + k_z v_z \sigma_z + k_x u_x \sigma_0. \quad (4)$$

Here  $\sigma_{x,y,z}$  are Pauli matrices and  $\sigma_0$  is the identity. The finite tilt  $u_x$  term does not change the Berry curvature but affects the Fermi surface shape and is crucial to get a finite Berry dipole. For  $\lambda > 0$ , this model describes an insulator of gap  $\Delta = (\lambda/|m|)$ . The critical point between this insulator and a Weyl semimetal is at  $\lambda = 0$ . In BiTeI, there are six pairs of Weyl points related by discrete  $C_{3v}$  operations and time reversal symmetry [3]. This model captures only one such pair but notice that all the pairs contribute additively to the total Berry dipole [38].

Assuming we have a finite carrier density  $n$  in the conduction band, and far away from the critical point such that  $\Delta$  is the largest energy scale and the tilt is small  $u_x \ll v_x$ , the dipole resulting from the long wavelength Hamiltonian Eq. (4) is

$$d_z \approx -\frac{nv_z u_x}{mv_x \Delta^2}. \quad (5)$$

Thus, as the transition is approached from the topological insulator side, the Berry dipole is strongly enhanced, with an asymptotic behavior as  $\sim 1/\Delta^2$  for large  $\Delta$ . The inset in Fig. 3 shows a direct comparison of this analytical result with the full band structure calculations in the low density regime. For sufficiently large  $\Delta$ , the numerical data are indeed consistent with the inverse quadratic behavior, which saturates when  $\Delta$  is reduced to values of the order of  $\mu$ .

The Weyl phase occurs for  $\lambda < 0$ . The distance between the Weyl nodes is  $2k_0$ , with  $k_0 = \sqrt{|\lambda|}$ . When the transition is approached from the Weyl phase, the dipole to leading order in  $u_x$  and  $k_0$ , and for  $k_0 \rightarrow k_F$ , is

$$d_z \approx -\frac{nu_x v_x v_z}{2k_0 \mu^2 v_y} \left(1 - \frac{v_y^2}{v_x^2}\right), \quad (6)$$

where  $v_y = k_0/m$  is the Fermi velocity along  $\hat{\mathbf{y}}$  near the Weyl point and  $k_F$  the Fermi momentum. We thus see that the dipole is enhanced as  $\sim 1/k_0$  as the Weyl points approach each other [39].

Notice that  $d_z$  is always finite provided that there is a finite Fermi surface. In particular, in the Weyl phase there is no divergence even when the chemical potential is at the nodes [40].

A similar analysis can be performed when the transition is approached from the trivial insulator side. The detailed argumentation differs slightly due to a different little group at the point where the conduction and valence bands touch [3,4], but an analogous model can be developed. The opposite Berry-dipole sign in this phase can be understood to arise from the different sign of the effective parameter  $m$  which controls the relative ordering in momentum space of the Weyl nodes with opposite chirality. This suggests that in other polar materials, like those studied in Ref. [3], in which the topological phase transitions occur through a similar Weyl nodes dynamics, or in Ref. [41], where the Weyl nodes ordering is reversed with an electric field, a change of sign in the Berry dipole can be expected as well.

*Experimental signatures.*—In the following, we describe different types of optoelectronic and transport measurements that can be used to probe the Berry dipole in BiTeI. Throughout this discussion we consider an electric field of frequency smaller than the interband optical threshold  $\omega \ll \Delta$ . Following Ref. [9], we expect a rectified current at zero frequency and a second harmonic current at  $2\omega$  given by, respectively

$$\mathbf{j}_0 = \frac{e^3 \tau}{2(1 + i\omega\tau)} \mathbf{E}^* \times (\mathbf{d} \times \mathbf{E}), \quad (7)$$

$$\mathbf{j}_{2\omega} = \frac{e^3 \tau}{2(1 + i\omega\tau)} \mathbf{E} \times (\mathbf{d} \times \mathbf{E}). \quad (8)$$

Here the fields  $\mathbf{E}$  are complex vectors to account for nontrivial light polarization. The formula can also be used to obtain currents in the dc limit by simply taking  $\mathbf{E}$  to be a real vector and multiplying, e.g., the result for  $\mathbf{j}_0$  by a factor of 2 [9].

The electric field polarization can be used to control the direction of  $\mathbf{j}_0$  and  $\mathbf{j}_{2\omega}$  and their relative amplitude. There are a few special cases of particular interest, the first of which is circularly polarized light. If the polarization plane is orthogonal to the polar axis,  $\mathbf{E} = E(\hat{\mathbf{x}} + i\hat{\mathbf{y}})$ ,  $\mathbf{j}_{2\omega}$  vanishes and the current reduces to

$$\mathbf{j}_0 = \frac{e^3 \tau d_z E^2 \hat{\mathbf{z}}}{2(1 + i\omega\tau)}. \quad (9)$$

In contrast, if the polarization plane contains the polar axis,  $\mathbf{E} = E(\hat{\mathbf{x}} + i\hat{\mathbf{z}})$ ,  $\mathbf{j}_0$  and  $\mathbf{j}_{2\omega}$  have equal amplitude but flow along different directions

$$\mathbf{j}_0 = \frac{e^3 \tau d_z E^2 (\hat{\mathbf{z}} + \hat{\mathbf{x}})}{2(1 + i\omega\tau)}, \quad \mathbf{j}_{2\omega} = \frac{e^3 \tau d_z E^2 (\hat{\mathbf{z}} - \hat{\mathbf{x}})}{2(1 + i\omega\tau)}. \quad (10)$$

It is remarkable that the currents flow along orthogonal directions that are 45 degrees away from the polar axis. Finally, for linearly polarized light with the electric field at an angle  $\theta$  from the polar axis,  $\mathbf{E} = E(\sin\theta\hat{\mathbf{x}} + \cos\theta\hat{\mathbf{z}})$ , the currents read

$$\mathbf{j}_0 = \mathbf{j}_{2\omega} = \frac{e^3 \tau d_z E^2 \sin\theta}{2(1 + i\omega\tau)} (\sin\theta\hat{\mathbf{z}} - \cos\theta\hat{\mathbf{x}}). \quad (11)$$

Notice that the  $\hat{\mathbf{x}}$  and  $\hat{\mathbf{z}}$  current components have different characteristic dependencies on  $\theta$ .

In summary, we have demonstrated that the Berry curvature dipole in BiTeI conveys key information about the topological state of the system. The Berry-dipole vector presents opposite orientations in the topologically distinct insulating phases. In addition, its magnitude sharply peaks at the phase boundaries between the insulating phases and the intervening Weyl semi-metallic phase. Optoelectronics and transport measurements, such as the nonlinear Hall effect, are predicted to offer direct experimental evidence of the topological phase transitions in this material under pressure.

We thank Ulrike Nitzsche for technical assistance. J. v. d. B. acknowledges support from the German Research Foundation (DFG) via SFB 1143. We are thankful to Snehasish Nandy for discussions and to Liang Fu for suggesting BiTeI as a promising platform to study the Berry curvature dipole.

- 
- [1] K. Ishizaka, M. S. Bahramy, H. Murakawa, M. Sakano, T. Shimojima, T. Sonobe, K. Koizumi, S. Shin, H. Miyahara, A. Kimura *et al.*, Giant Rashba-type spin splitting in bulk BiTeI, *Nat. Mater.* **10**, 521 (2011).
  - [2] M. S. Bahramy, B.-J. Yang, R. Arita, and N. Nagaosa, Emergence of non-centrosymmetric topological insulating phase in BiTeI under pressure, *Nat. Commun.* **3**, 679 (2012).
  - [3] J. Liu and D. Vanderbilt, Weyl semimetals from noncentrosymmetric topological insulators, *Phys. Rev. B* **90**, 155316 (2014).
  - [4] I. P. Rusinov, T. V. Menshchikova, I. Yu. Sklyadneva, R. Heid, K.-P. Bohnen, and E. V. Chulkov, Pressure effects on crystal and electronic structure of bismuth tellurohalides, *New J. Phys.* **18**, 113003 (2016).
  - [5] Y. Qi, W. Shi, P. G. Naumov, N. Kumar, R. Sankar, W. Schnelle, C. Shekhar, F.-C. Chou, C. Felser, B. Yan, and S. A. Medvedev, Topological quantum phase transition and superconductivity induced by pressure in the bismuth tellurohalide BiTeI, *Adv. Mater.* **29**, 1605965 (2017).

- [6] X. Xi, C. Ma, Z. Liu, Z. Chen, W. Ku, H. Berger, C. Martin, D. B. Tanner, and G. L. Carr, Signatures of a Pressure-Induced Topological Quantum Phase Transition in BiTeI, *Phys. Rev. Lett.* **111**, 155701 (2013).
- [7] M. K. Tran, J. Levallois, P. Lerch, J. Teyssier, A. B. Kuzmenko, G. Autès, O. V. Yazyev, A. Ubaldini, E. Giannini, D. van der Marel, and A. Akrap, Infrared- and Raman-Spectroscopy Measurements of a Transition in the Crystal Structure and a Closing of the Energy Gap of BiTeI Under Pressure, *Phys. Rev. Lett.* **112**, 047402 (2014).
- [8] D. VanGennep, A. Linscheid, D. E. Jackson, S. T. Weir, Y. K. Vohra, Helmuth Berger, G. R. Stewart, R. G. Hennig, P. J. Hirschfeld, and J. J. Hamlin, Pressure-induced superconductivity in the giant Rashba system BiTeI, *J. Phys. Condens. Matter* **29**, 09LT02 (2017).
- [9] Inti Sodemann and Liang Fu, Quantum nonlinear Hall Effect Induced by Berry Curvature Dipole in Time-Reversal Invariant Materials, *Phys. Rev. Lett.* **115**, 216806 (2015).
- [10] Joel E. Moore and J. Orenstein, Confinement-Induced Berry Phase and Helicity-Dependent Photocurrents, *Phys. Rev. Lett.* **105**, 026805 (2010).
- [11] E. Deyo, L. E. Golub, E. L. Ivchenko, and B. Spivak, Semiclassical theory of the photogalvanic effect in non-centrosymmetric systems, [arXiv:0904.1917v1](https://arxiv.org/abs/0904.1917v1).
- [12] T. Low, Y. Jiang, and F. Guinea, Topological currents in black phosphorus with broken inversion symmetry, *Phys. Rev. B* **92**, 235447 (2015).
- [13] F. de Juan, A. G. Grushin, T. Morimoto, and J. E. Moore, Quantized circular photogalvanic effect in Weyl semimetals, *Nat. Commun.* **8**, 15995 (2017).
- [14] H. B. Banks, Q. Wu, D. C. Valocin, S. Mack, A. C. Gossard, L. Pfeiffer, R.-B. Liu, and M. S. Sherwin, Dynamical Birefringence: Electron-Hole Recollisions as Probes of Berry Curvature, *Phys. Rev. X* **7**, 041042 (2017).
- [15] T. T. Luu and H. J. Wörner, Measurement of the Berry curvature of solids using high-harmonic spectroscopy, *Nat. Commun.* **9**, 916 (2018).
- [16] L. P. Gavensky, G. Usaj, and C. A. Balseiro, Photo-electrons unveil topological transitions in graphene-like systems, *Sci. Rep.* **6**, 36577 (2016).
- [17] Q. Ma, S.-Y. Xu, H. Shen, D. Macneill, V. Fatemi, A. M. Mier Valdivia, S. Wu, T.-R. Chang, Z. Du, C.-H. Hsu *et al.*, Observation of the nonlinear Hall effect under time reversal symmetric conditions, [arXiv:1809.09279](https://arxiv.org/abs/1809.09279).
- [18] K. Kang, T. Li, E. Sohn, J. Shan, and K. F. Mak, Observation of the nonlinear anomalous Hall effect in 2D WTe<sub>2</sub>, [arXiv:1809.08744](https://arxiv.org/abs/1809.08744).
- [19] S.-Y. Xu, Q. Ma, H. Shen, V. Fatemi, S. Wu, T.-R. Chang, G. Chang, A. M. Mier Valdivia, C.-K. Chan, Q. D. Gibson *et al.*, Electrically switchable Berry curvature dipole in the monolayer topological insulator WTe<sub>2</sub>, *Nat. Phys.* **14**, 900 (2018).
- [20] J.-S. You, S. Fang, S.-Y. Xu, E. Kaxiras, and T. Low, Berry curvature dipole current in the transition metal dichalcogenides family, *Phys. Rev. B* **98**, 121109 (2018).
- [21] Y. Zhang, J. van den Brink, C. Felser, and B. Yan, Electrically tuneable nonlinear anomalous Hall effect in two-dimensional transition-metal dichalcogenides WTe<sub>2</sub> and MoTe<sub>2</sub>, *2D Mater.* **5**, 044001 (2018).
- [22] L.-k. Shi and J. C. W. Song, Berry curvature switch and magneto-electric effect in WTe<sub>2</sub> monolayer, [arXiv:1805.00939](https://arxiv.org/abs/1805.00939).

- [23] We used WIEN2K [24] with the GGA functional, a  $24^3$   $k$ -mesh, and setting  $R_{MT} = 2.5$  and  $K_{\max} = 8.5R_{MT}^{-1}$ .
- [24] P. Blaha, K. Schwarz, G. K. H. Madsen, D. Kvasnicka, J. Luitz, R. Laskowski, F. Tran, and L. D. Marks, *WIEN2k, An Augmented Plane Wave + Local Orbitals Program for Calculating Crystal Properties* (Karlheinz Schwarz, Techn. Universität Wien, Austria, 2018), ISBN 3-9501031-1-2.
- [25] For each pressure we built maximally localized Wannier functions for  $p$  orbitals of Bi, Te, and I [26,27] and computed  $\Omega_{n,d}$  by Wannier interpolation [28] and  $D_{bd}$  as  $\int [d^3k/(2\pi)^3] \sum_n [\partial\Omega_{n,d}/\partial k_n] f_0(E_{n\mathbf{k}})$  using a  $1000 \times 1000 \times 300$  mesh in the Brillouin-zone region that contains the conducting states in the range of doping analyzed. We also performed calculations with FPLO [29] based on which we found the same evolution of  $\Omega_{n,d}$  with  $P$  [30].
- [26] J. Kuneš, R. Arita, P. Wissgott, A. Toschi, H. Ikeda, and K. Held, Wien2wannier: From linearized augmented plane waves to maximally localized Wannier functions, *Comput. Phys. Commun.* **181**, 1888 (2010).
- [27] A. A. Mostofi, J. R. Yates, G. Pizzi, Y.-S. Lee, I. Souza, D. Vanderbilt, and N. Marzari, An updated version of wannier90: A tool for obtaining maximally-localised Wannier functions, *Comput. Phys. Commun.* **185**, 2309 (2014).
- [28] X. Wang, J. R. Yates, I. Souza, and D. Vanderbilt, Ab initio calculation of the anomalous Hall conductivity by Wannier interpolation, *Phys. Rev. B* **74**, 195118 (2006).
- [29] K. Koepf and H. Eschrig, Full-potential nonorthogonal local-orbital minimum-basis band-structure scheme, *Phys. Rev. B* **59**, 1743 (1999).
- [30] See Supplemental Material at <http://link.aps.org/supplemental/10.1103/PhysRevLett.121.246403>, which includes Refs. [31–35], for (i) Berry-dipole dependence on  $\mu$ , (ii) discussion of DFT calculations, and (iii) formulae associated with the model.
- [31] J. Kuneš, P. Novák, R. Schmid, P. Blaha, and K. Schwarz, Electronic structure of fcc Th: Spin-orbit calculation with  $6p_{1/2}$  local orbital extension, *Phys. Rev. B* **64**, 153102 (2001).
- [32] M. S. Bahramy, R. Arita, and N. Nagaosa, Origin of giant bulk Rashba splitting: Application to BiTeI, *Phys. Rev. B* **84**, 041202 (2011).
- [33] M. Sakano, J. Miyawaki, A. Chainani, Y. Takata, T. Sonobe, T. Shimojima, M. Oura, S. Shin, M. S. Bahramy, R. Arita, N. Nagaosa, H. Murakawa, Y. Kaneko, Y. Tokura, and K. Ishizaka, Three-dimensional bulk band dispersion in polar BiTeI with giant Rashba-type spin splitting, *Phys. Rev. B* **86**, 085204 (2012).
- [34] I. P. Rusinov, I. A. Nechaev, S. V. Eremeev, C. Friedrich, S. Blügel, and E. V. Chulkov, Many-body effects on the Rashba-type spin splitting in bulk bismuth tellurohalides, *Phys. Rev. B* **87**, 205103 (2013).
- [35] S. Güler-Kılıç and Ç. Kılıç, Pressure dependence of the band-gap energy in BiTeI, *Phys. Rev. B* **94**, 165203 (2016).
- [36] Y. Zhang, Y. Sun, and B. Yan, Berry curvature dipole in Weyl semimetal materials: An ab initio study, *Phys. Rev. B* **97**, 041101 (2018).
- [37] S. S. Tsirkin, P. A. Punte, and I. Souza, Gyrotropic effects in trigonal tellurium studied from first principles, *Phys. Rev. B* **97**, 035158 (2018).
- [38] Weyl points pairs related by  $C_3$  naturally contribute equally to  $d_z$ . Those related by time reversal also contribute equally because  $\Omega$  is odd under time reversal but its curl is even.
- [39] Further details of the Weyl semimetal materials will appear in a forthcoming publication.
- [40] This follows from Eq. (6) because within the Weyl semimetal phase  $n \propto \mu^3$ . In terms of  $\mu$ , the Berry dipole in this regime reads  $d_z \approx -(4\pi\mu u_x/3k_0 v_y^2)[1 - (v_y^2/v_x^2)]$  and vanishes when  $\mu \rightarrow 0$ .
- [41] S. Singh, A. C. Garcia-Castro, I. Valencia-Jaime, F. Muñoz, and A. H. Romero, Prediction and control of spin polarization in a Weyl semimetallic phase of BiSb, *Phys. Rev. B* **94**, 161116 (2016).